Comprehensive measurement model of geometric errors for three linear axes of computer numerical control machine tools

OPEN ACCESS
IOP Publishing
Measurement Science and Technology
Meas. Sci. Technol. **33** (2022) 015202 (18pp)
https://doi.org/10.1088/1361-6501/ac2dbb

Comprehensive measurement model of geometric errors for three linear axes of computer numerical control machine tools

Peizhi Jia, Bin Zhang, Fajia Zheng and Qibo Feng*

KeyLaboratory of Luminescence and Optical Information, Ministry of Education, Beijing Jiaotong University, Beijing 100044, People's Republic of China

E-mail: qbfeng@bjtu.edu.cn

Received 8 July 2021, revised 21 September 2021
Accepted for publication 7 October 2021
Published 21 October 2021

Abstract

The geometric error measurement of computer numerical control (CNC) machine tools is developing towards automation and high precision. This not only improves the measurement efficiency, but also reduces the error caused by the long measurement time. This paper proposes a high-efficiency, automatic method of measuring 21 geometric errors of the three linear axes of CNC machine tools and establishes a comprehensive measurement model. The measurement system and model are applicable to linear axis geometric error measurement for all CNC machine tools. The measurement model was developed using rigid body kinematics theory and combined with the ray-tracing method. It mainly analyses the error crosstalk, system errors caused by optical components, laser beam drift, and non-parallelism errors between the measuring beams. ZEMAX was used to verify the model accuracy. Further, repeatability and comparison experiments were conducted to confirm the reliability and accuracy of the measurement system and model.

Keywords: geometric error, computer numerical control machine tool, linear axis, measurement model

(Some figures may appear in colour only in the online journal)

Abbreviations

BS	beam splitter
CCR	corner cube retroreflector
CNC	computer numerical control
D	detector
DOF	degree of freedom
HTM	homogeneous coordinate transformation matrix
HWP	half-wave plate
P	polarizer
PBS	polarized beam splitter
PSD	position-sensitive detector
QD	quadrant detector
QWP	quarter-wave plate
RAP	right angle prism

* Author to whom any correspondence should be addressed.

1. Introduction

The rapid development of the manufacturing industry and improvement in processing level have imposed increasingly high requirements on the processing accuracy of CNC machine tools. At present, the main method of improving the accuracy of CNC machine tools is error compensation [1–4]. As a prerequisite for error compensation, the geometric error measurement of CNC machine tools is developing toward automation and high precision. This not only improves the measurement efficiency, but also reduces the error caused by the long measurement time. Therefore, many scholars around the world have carried out extensive and in-depth research on the measurement of geometric error of CNC machine tools.

According to the definition in ISO230-1, the linear guide has 6DOF geometric errors. Three-axis CNC machine tools have 21 geometric errors. Whereas five-axis CNC machine tools have 42 geometric errors in total, of which 21 are from the three linear axes. In addition, according to the research of Mayer *et al* [5], the kinematic error of the linear axis is the result of the combined effect of various geometric errors of the guide rail on which the slider moves at the same time. In the process of geometric error measurement, the measurement result is usually cross talked by other geometric errors, so the measurement result is not purely geometric error but motion error. The measurement result is geometric error or motion error usually depends on the measurement method.

The measurement method of linear axis geometric error mainly includes direct and indirect measurement method. Indirect measurement method includes the use of workpiece tests [6, 7], R-tests [8, 9], 3D laser ball bars [10], and laser trackers [11–14]. Some scholars obtain the individual geometric errors by decoupling after measuring the volumetric errors based on the principle of laser interference [15]. Indirect measurement methods usually do not directly obtain various geometric errors. The single geometric error needs to be decoupled through the kinematic error model. Laser interferometry is a typical direct measurement method [16–18]. The direct measurement method usually directly measures each individual geometric error according to the definition. ISO230-1 recommends using a laser interferometer to measure the multi-degree-of-freedom geometric errors of a linear axis. However, efficiency is a key issue for measuring 21 geometric errors of three linear axes based on the principle of interference. Moreover, the measurement accuracy is extremely susceptible to long-term environmental changes, reducing the overall accuracy. To improve the measurement efficiency, various methods of simultaneously measuring the 6DOF geometric errors of the linear axes of machine tools have been extensively studied, including methods based on the combination of laser interferometry and laser collimation [19–21], laser collimation [22, 23], surface encoders [24, 25], and diffraction gratings [26–28]. In addition, some commercial instruments have been developed, including API 5D/6D measuring instrument and Renishaw laser 6D simultaneous measurement system. Both JEANer Meßtechnik GmbH and Zygo proposed a multi-axis laser interferometer system that can simultaneously measure the partial geometric errors of multi linear axes. In these methods, it is necessary to re-install and re-adjust the instruments, and some errors cannot be measured.

To achieve quick and accurate measurement of the geometric errors of the linear axes of CNC machine tools, our research team proposed a series of measurement systems to direct measure simultaneously the 6DOF geometric error of a single linear axis [29–32]. A novel method for automatically measuring 21 geometric errors of the three linear axes of CNC machine tools with one-step installation was proposed, and a corresponding measurement system was developed [33, 34]. Furthermore, the differences between the two measurement modes were analyzed [35]. However, the measurement system is complicated owing to the addition of a beam-steering unit. Further, it is necessary to analyze the influence of systemic errors on the measurement accuracy. Owing to the diversity of CNC machine tool types, the measurement system and model do not have universal adaptability. Therefore, this paper proposes simple beam-controlling and target units. In addition, it establishes a comprehensive measurement model based on rigid body kinematics theory and the ray tracing method. The measurement system and comprehensive measurement model have universal applicability to the linear axis geometric errors measurement of all types of CNC machine tools.

In summary, based on the previously proposed linear axis 6DOF geometric error measurement system, we designed and developed new beam-controlling and target units that can automatically measure 21 geometric errors of three linear axes. Section 2 describes the principle and configuration of the measurement system. Section 3 establishes a comprehensive measurement model. The model mainly analyses the crosstalk, manufacturing, installation errors of the optical components and non-parallelism errors between two measuring beams. ZEMAX software was used to simulate some key measurement models numerically in section 4. Section 5 presents the repeatability, comparison experiments and the measurement of 21 geometric errors of three-axis CNC machine tools using the proposed system. Finally, section 6 provides the conclusions.

2. Measurement principles and measurement system configuration

This section mainly introduces the measurement principle and system configuration of the system. In section 2.1, the Y-axis measurement is taken as an example to describe in detail the propagation of the measurement beam in the measurement unit, the beam control unit and the target unit, and explain the measurement principle. In section 2.2, the components of the measurement system are introduced in detail. Combined with the machine tool, the measurement procedures of 21 geometric errors of three linear axes are described separately. In the last part, the pre-adjustment method of the beam control unit is introduced.

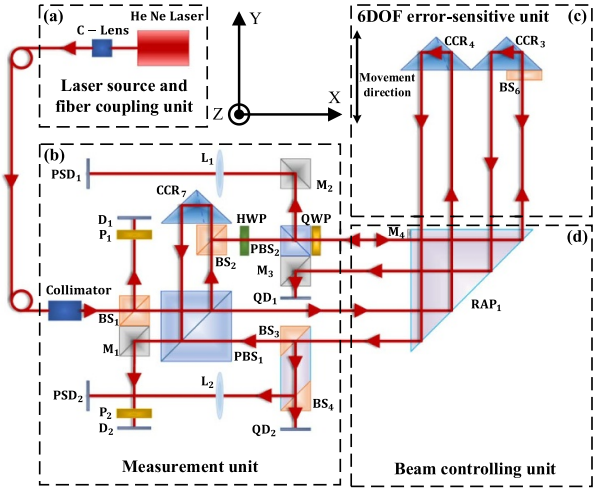

Figure 1. Optical configuration for all geometric errors of the Y-axis.

2.1. Principle of linear axis 6DOF geometric error measurement

Figure 1 shows the optical configuration used to measure the total geometric errors of the Y-axis. The 6DOF error-sensitive unit is composed of two CCRs and BS film. The linearly polarized light generated by the dual-frequency laser is coupled to the polarization maintaining fiber as the light source of the measurement system.

The collimated beam after the collimator is divided into two measuring beams by PBS1 and BS2. One is reflected by BS6 and CCR3 after being reflected by RAP1. The other is reflected by RAP1 and then reflected by CCR4. The two measuring beams return to the measurement unit after reflection, and irradiate different detectors after being split. The positioning error is measured based on the principle of heterodyne interferometry, and calculated with the signals of the detectors D1 and D2. The straightness error is measured based on the principle of collimation, and obtained from the signal of the detector QD1. Pitch and yaw are measured based on the principle of autocollimation, and obtained from the signal of the detector PSD1. Roll is calculated based on the vertical variation of the light spot on the detectors QD1 and QD2. The angle drift of the measuring beam is calculated with the signal of PSD2 to compensate the influence on the measurement accuracy. Ideally, the measurement model of the 6DOF geometric errors of the Y-axis can be expressed as [30]

$$\begin{aligned}
\delta_{yy} &= \frac{\lambda\Delta\phi}{4n\pi} - L' \\
\delta_{xy} &= \frac{\Delta Y_{\mathrm{QD1}}}{2} \pm L\frac{\Delta Y_{\mathrm{PSD2}}}{f} \\
\delta_{xy} &= \frac{\Delta Y_{\mathrm{QD1}}}{2} \pm L\frac{\Delta Y_{\mathrm{PSD2}}}{f} \\
\varepsilon_{zy} &= \frac{\Delta Y_{\mathrm{PSD1}}}{2f} \pm \frac{\Delta Y_{\mathrm{PSD2}}}{f} \\
\varepsilon_{xy} &= \frac{\Delta Z_{\mathrm{PSD1}}}{2f} \pm \frac{\Delta Y_{\mathrm{PSD2}}}{f} \\
\varepsilon_{yy} &= \frac{\Delta Z_{\mathrm{QD2}} - \Delta Z_{\mathrm{QD1}}}{2h}.
\end{aligned} \tag{1}$$

Here, λ is the wavelength; $\Delta\phi$ is the phase difference between the measured and reference beams; L' is the displacement of the Y-axis; ΔY_{QD1} and ΔZ_{QD1} are the horizontal and vertical displacement changes of the spot on detector QD1, respectively; ΔY_{PSD1} and ΔZ_{PSD1} are the horizontal and vertical displacement changes of the spot on detector PSD1, respectively; f is the focal length of lens L_1 and L_2; ΔZ_{QD2} is the vertical displacement change of the spot on detector QD2; and h is the distance between the two measuring beams. In addition, without considering the system error and measurement mode, the measurement models of the X- and Z-axes are the same as that of the Y-axis.

2.2. Measurement system configuration

Figure 2 shows the system configuration for measuring all geometric errors of three linear axes. The measurement system consists of a laser source and fiber coupled unit, measurement unit, target unit, beam controlling unit and linear translation stage. The measurement unit and linear translation stage are fixed on the Invar base plate, and the beam controlling unit is connected to the linear translation stage through an angle adjustment mechanism. A target unit that is sensitive to 18 geometric errors of the three linear axes is fixed on a spindle. Target unit mainly includes three mutually perpendicular 6DOF error-sensitive units, which correspond to measuring the 6DOF geometric errors of the X-, Y-, and Z-axes. The beam controlling unit consists of two RAPs and an optical flat crystal.

Based on the principle of simultaneous measurement of 6DOF geometric errors of the linear axes, one-step installation and automatic measurement of 21 geometric errors of the three linear axes of CNC machine tools can be achieved by adding a beam controlling unit. Firstly, the beam controlling unit is moved out of the optical path. Then, the angle of the measurement unit is adjusted to make the measurement beam parallel to the X-axis. The target unit is adjusted such that the measurement beam returns to the center of the detector. Figure 3(a) shows the measurement process of the X-axis geometric error. Secondly, right angle prisms RAP1 and RAP2 are moved into the optical path completely, and the measurement beams are parallel to the Y- and Z-axes, respectively, after being turned. Figures 3(b) and (c) shows the measurement process of the Y- and Z-axis 6DOF geometric errors, respectively. The measurement can be conducted point by point, and the 6DOF geometric errors of all measuring points on the three linear axes can be obtained. Based on the straightness error of every measurement point on the X-, Y-, and Z-axes, three fitting axes were obtained. Finally, the squareness error of each pair of axes was

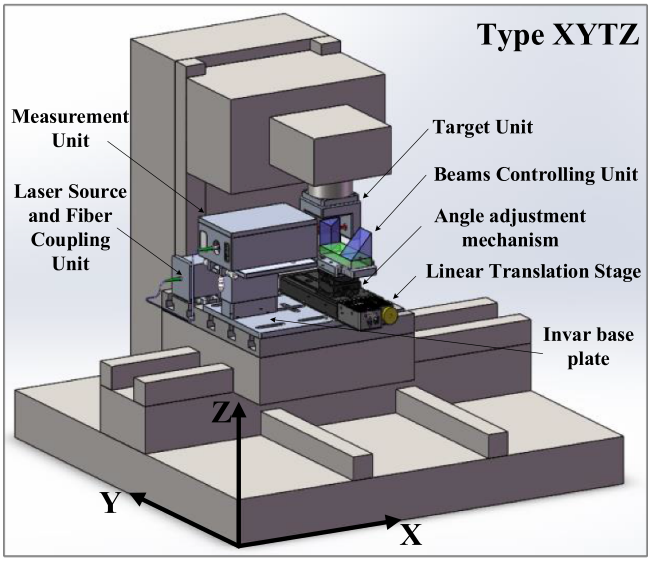

Figure 2. System configuration.

calculated based on these fitting lines. Ultimately, 21 geometric errors of the three linear axes of the machine tool were obtained.

In addition, in order to achieve precise 90° control of the beam, the angle adjustment mechanism can be adjusted so that the incident beam is perpendicular to the incident surface of the RAP. Figure 4 shows the adjustment principle of the beam control unit. By adjusting the angle adjustment mechanism under the beam control unit, the angle measuring beam is returned to the center of the detector PSD1. At this time, the measuring beam is perpendicular to the beam control unit. The reflected beam of the RAP is perpendicular to the incident beam. The 90° included angle is used as a reference for squareness error measurement.

3. Measurement model for geometric errors

The 6DOF geometric errors of each linear axis and plus the three squareness errors between the three linear axes yields a total of 21 motion errors for a three-axis CNC machine tool, as listed in table 1. The geometric error of the CNC machine tools is expressed as the motion error δ_{uv} along the coordinate axis and rotation angle error ε_{uv} around the coordinate axis. The first subscript indicates the error direction, and the second subscript indicates the axis to be measured. The positioning error of the linear axis is measured by a dual-frequency laser interferometer; this measurement model is not discussed here. Other geometric error measurement models were established in this study based on the rigid body kinematics theory and ray tracing method. This section introduces the method of establishing the measurement model and presents the final model. The measurement model was applied to process raw system data. The measurement system and comprehensive measurement model can be used to measure the geometric errors of the linear axes of all types of CNC machine tools.

3.1. Method of establishing the measurement model

A comprehensive measurement model was established using standard homogeneous coordinate transformation, combined with the closed-loop characteristics of the connection chain between the measurement and target units. Consider the Y-axis 6DOF geometric error measurement of the XYTZ-type CNC machine tool as an example. As shown in figure 5, a reference coordinate system R was established on the pedestal of the machine tool, and local coordinate systems on the X-, Y-, and Z-axes; spindle; measurement unit; RAP; Invar base plate; and CCR were also established. The directions of the local and reference coordinate systems were the same.

The transformation matrix between each coordinate system was established according to the principle of homogeneous coordinate transformation. The elements in the HTM represent some of the systematic or geometric errors. The Invar substrate and measurement unit are rigidly connected, and there is no relative angular or position change, so HTM ${}^{M}_{R_{MA}}T$ is the identity matrix. The RAP is connected to the Invar substrate through a linear guide, so the position and angular will change. Therefore, HTM ${}^{R_{MA}}_{A}T$ from the Invar substrate coordinate system R_{MA} to the RAP coordinate system A includes the position and angular errors of the RAP. ${}^{R_{MA}}_{A}T$ can be expressed as:

$$ {}^{R_{MA}}_{A}T = \begin{pmatrix} 1 & -\varepsilon_{yir} & \varepsilon_{xir} & \delta_{xir} \\ \varepsilon_{yir} & 1 & -\varepsilon_{zir} & \delta_{yir} \\ -\varepsilon_{xir} & \varepsilon_{zir} & 1 & \delta_{zir} \\ 0 & 0 & 0 & 1 \end{pmatrix} . \qquad (2) $$

ε_{xir}, ε_{yir}, and ε_{zir} are the angular errors of the RAP, and δ_{xir}, δ_{yir}, and δ_{zir} are its position errors.

Because there is no relative movement between the Invar substrate and X-axis, the HTM from the Invar substrate coordinate system R_{MA} to the X-axis coordinate system is the identity matrix. Similarly, HTM ${}^{X}_{Y}T$ from the X-axis coordinate system to the Y-axis coordinate system is the identity

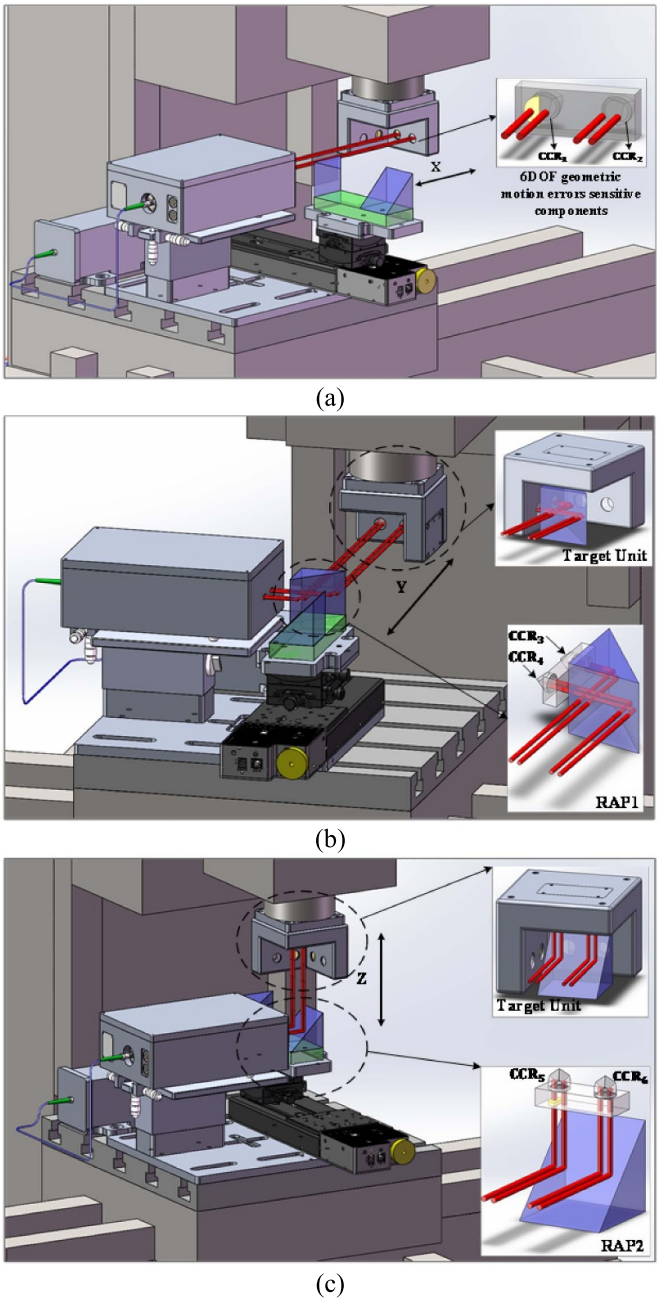

Figure 3. Measurement process. (a) *X*-axis measurement process; (b) *Y*-axis measurement process; (c) *Z*-axis measurement process.

matrix. When performing the *Y*-axis measurement, HTM ${}^{Y}_{R}T$ between the *Y*-axis coordinate system and machine reference coordinate system *R* contains the 6DOF geometric errors of the *Y*-axis. The HTM can be expressed as

$$ {}^{Y}_{R}T = \begin{pmatrix} 1 & -\varepsilon_{yy} & \varepsilon_{xy} & \delta_{xy} \\ \varepsilon_{yy} & 1 & -\varepsilon_{zy} & L+\delta_{yy} \\ -\varepsilon_{xy} & \varepsilon_{zy} & 1 & \delta_{zy} \\ 0 & 0 & 0 & 1 \end{pmatrix}. \tag{3} $$

Similarly, there is no relative movement between the pedestal and *Z*-axis, *Z*-axis and spindle; thus, HTM ${}^{R}_{Z}T$ and ${}^{Z}_{S}T$ are both identity matrices. The measuring unit, RAP, and Invar base plate were integrated as a whole. Taking this whole as a reference, the installation error of the measurement system was superimposed on the CCR. Owing to the installation error between the CCR and spindle, HTM ${}^{S}_{C}T$ can be expressed as

$$ {}^{S}_{C}T = \begin{pmatrix} 1 & -\varepsilon_{yic} & \varepsilon_{xic} & \delta_{xic} \\ \varepsilon_{yic} & 1 & -\varepsilon_{zic} & \delta_{yic} \\ -\varepsilon_{xic} & \varepsilon_{zic} & 1 & \delta_{zic} \\ 0 & 0 & 0 & 1 \end{pmatrix}. \tag{4} $$

δ_{xic}, δ_{yic}, and δ_{zic} represent the installation position errors of the CCR, and ε_{xic}, ε_{yic}, and ε_{zic} represent its installation angle errors.

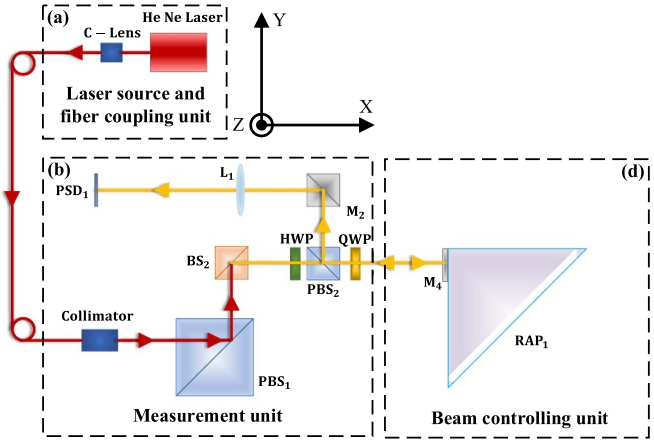

Figure 4. The adjustment principle of the beam-controlling unit.

Table 1. 21 geometric errors of three-axis CNC machine tools.

Geometric error	*X*-axis	*Y*-axis	*Z*-axis
Position error	δ_{xx}	δ_{yy}	δ_{zz}
Horizontal straightness	δ_{yx}	δ_{xy}	δ_{yz}
Vertical straightness	δ_{zx}	δ_{zy}	δ_{xz}
Yaw	ε_{zx}	ε_{zy}	ε_{xz}
Pitch	ε_{yx}	ε_{xy}	ε_{yz}
Roll	ε_{xx}	ε_{yy}	ε_{zz}
Squareness error		S_{xy}, S_{xz}, S_{yz}	

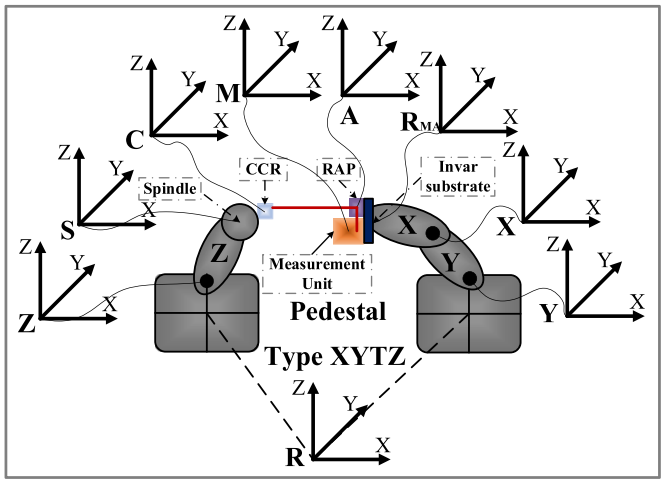

Figure 5. Establishment of the integrated coordinate system of the machine tool and measurement system.

The measurement beam expression in the measurement unit coordinate system was established. Taking one measurement beam as the reference, two non-parallelism errors, ε_{PEz} and ε_{PEy}, were introduced into the expression of the second measurement beam. From the measurement unit to the RAP coordinate system, HTM ${}^{M}_{A}T = {}^{M}_{R_{MA}}T \cdot {}^{R_{MA}}_{A}T$ could be used to obtain the expression of the measurement beams in the RAP coordinate system. The transmission and reflective surfaces of the RAP were regarded as space planes. The key information was the normal vector and expression of the plane. This information includes manufacturing errors. ε_{zmrs1}, ε_{ymrs1}, ε_{zmrs2}, and ε_{ymrs2} are the manufacturing errors between the two right-angled planes (S1 and S2) and reflective plane (S3), as shown in figure 6(a). The measurement beam was regarded as a straight line in space, and the key information was the direction vector and expression of the straight line. The intersection point coordinates could be obtained by combining the expressions of the plane and straight lines. By combining the direction vector of the straight line with the refraction or reflection matrix of each plane [31], the direction vector of the refracted or reflected beams could be determined. Finally, the space expression of the point normal of the beam was obtained. After the beams were refracted and reflected by the RAP, they were turned 90°. Then, through the transmission chain model, the measurement beam expression was converted from the RAP coordinate system to the CCR coordinate system, and participates in the CCR calculation.

Regarding the transmission surface of the CCR as a space plane, the key information is the normal vector and expression of the plane. Regarding the measurement beam as a straight line in space, the key information is the direction vector and expression of the straight line. By using the point-normal equation of the plane and point-direction equation of the line, the coordinates of the intersection point were calculated. The direction vectors of the refracted and reflected beams were determined by combining the direction vector of the straight line with the refraction and radiation matrices of each plane. Finally, the space expression of the point normal of the beam was obtained, and the expression for the beam reflected from the CCR was calculated. Ideally, the three reflecting surfaces

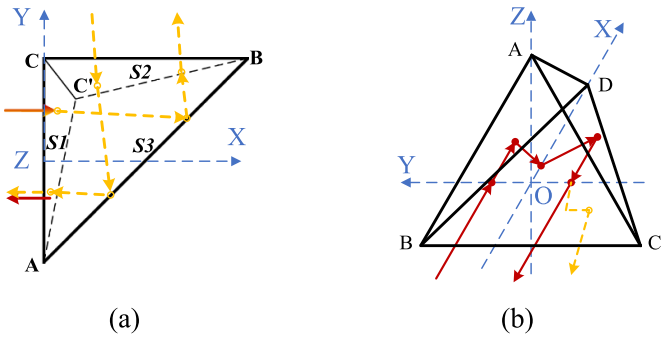

Figure 6. Modeling of (a) right angle prism and (b) CCR.

of a CCR are perpendicular to each other. However, owing to manufacturing errors, there are angular errors between these surfaces. Consequently, the incident and reflected beams are not parallel. As shown in figure 6(b), the intersection of the incident and outgoing beams with a transmission surface is asymmetric with respect to the vertex of the CCR. In the measurement model, the manufacturing error of the CCR is converted into the angular and displacement error between the outgoing beam and the incident beam. The angular and displacement errors were added to the direction vector and point coordinates of the outgoing beam, respectively. Finally, the reflected beam of the CCR carrying various system errors and geometric errors was obtained in the CCR coordinate system.

Convert the CCR reflected beam expression from the CCR coordinate system to the RAP coordinate system. Then, based on the ray tracing method, the reflected beam expression of RAP can be obtained. Finally, transform the RAP reflected beam expression from the RAP coordinate system to the measurement unit coordinate system. The coordinates of the spot on the detector are obtained by combining the expression of the return beam and the expression of the detector surface. The horizontal and vertical coordinates of the intersection are the final measurement model. Using the same modeling method, an angle error measurement model could be obtained.

To improve the adaptability of measurement system and model, the same method was used to establish comprehensive measurement models for other types of CNC machine tools. The analysis showed that there are two different measurement modes in the measurement process because of the different types of machine tools [33]. In general, the default measurement mode occurs when the target unit moves with the work table. There is also a measurement mode in which the target unit is fixed and the other parts move. When measuring the geometric error of the linear axis of CNC machine tool, it is only necessary to select the corresponding measurement model according to the measurement mode without considering the type of the machine tool. Therefore, the adaptability of the measurement system and comprehensive measurement model could be improved.

3.2. Measurement model

Firstly, a comprehensive measurement model was established based on the above method. Secondly, MATLAB was used to perform the correlation matrix product operations and simplify the measurement model. The number of higher orders was ignored in the model. Finally, measurement models of the X-, Y-, and Z-axes were obtained. Because there are two measurement modes in the machine tool measurement process, $i = 1$ was used to indicate the measurement mode with the target unit moving, and $i = 2$ was used to indicate the measurement mode with the target unit fixed and the other parts moving.

3.2.1. X-axis measurement model. Equation (5) shows the X-axis 5DOF geometric errors measurement model:

$$
\begin{aligned}
\delta_{yx} &= (-1)^{i-1}\left(\frac{\Delta Y_{\mathrm{QD1}}}{2} - \frac{\delta_{ymc1}}{2} + \frac{\varepsilon_{zmc1}}{2}L - \delta_{yic} + \frac{(\varepsilon_{zic}+\varepsilon_{zx})\left(6L_D+\sqrt{6}a\right)}{6n} + (i-1)(\varepsilon_{zx}L)\right) \pm L\frac{\Delta Y_{\mathrm{PSD2}}}{f}\\
\delta_{zx} &= (-1)^{i-1}\left(\frac{\Delta Z_{\mathrm{QD1}}}{2} - \frac{\delta_{zmc1}}{2} - \frac{\varepsilon_{ymc1}}{2}L - \delta_{zic} - \frac{(\varepsilon_{yic}+\varepsilon_{yx})\left(6L_D+\sqrt{6}a\right)}{6n} - (i-1)(\varepsilon_{yx}L)\right) \pm L\frac{\Delta Z_{\mathrm{PSD2}}}{f}\\
\varepsilon_{zx} &= (-1)^{2-i}\left(\frac{\Delta Y_{\mathrm{PSD1}}}{2f} + \varepsilon_{zic} - \frac{1}{2}\varepsilon_{PEz}\right) \pm \frac{\Delta Y_{\mathrm{PSD2}}}{f}\\
\varepsilon_{yx} &= (-1)^{i-1}\left(\frac{\Delta Z_{\mathrm{PSD1}}}{2f} - \varepsilon_{yic} + \frac{1}{2}\varepsilon_{PEy}\right) \pm \frac{\Delta Z_{\mathrm{PSD2}}}{f}\\
\varepsilon_{xx} &= (-1)^{i-1}\frac{\Delta Z_{\mathrm{QD1}} - \Delta Z_{\mathrm{QD2}} + 2\varepsilon_{PEy}\left(L + \frac{6L_D+\sqrt{6}a}{6n}\right) + \delta_{zmc2} - \delta_{zmc1} + L(\varepsilon_{ymc2} - \varepsilon_{ymc1})}{2h}.
\end{aligned}
\tag{5}
$$

In the above measurement model, δ_{ymc1} and δ_{zmc1} represent the position errors of the beam in the horizontal and vertical directions, respectively, caused by the manufacturing errors of CCR1. ε_{zmc1} and ε_{ymc1} represent the two non-parallel errors between the incident and retroreflected beams caused by the manufacturing errors of CCR1. δ_{zmc2} and ε_{ymc2} are the position error of the beam in the vertical direction caused by the manufacturing error of CCR2 and the angle error between the incident and retroreflected beams. a is the side length of the equilateral triangle that forms the base of the CCR. δ_{yic} and δ_{zic} represent the installation position errors of the CCR, and ε_{zic} and ε_{yic} represent the installation angle errors of the CCR. ε_{PEz} and ε_{PEy} are the non-parallelism errors between the two measurement beams. h is the distance between the two measurement beams. L_D is the thickness of the glass plate. The term $\sqrt{6}a/6n$ comes from the corner cube reflector, which contains size information a and refractive index n. The incident surface of the corner cube reflector is regarded as an equilateral triangle. a is the side length of an equilateral triangle.

3.2.2. Y-axis measurement model. Equation (6) shows the Y-axis 5DOF geometric errors measurement model. Because the beam controlling unit is added, the manufacturing errors of the RAP and the influence of the installation errors of the RAP on the measurement system are reflected in the model:

$$
\begin{aligned}
\delta_{xy} &= (-1)^{i-1}\left(\frac{\Delta Y_{\mathrm{QD1}}}{2} - \frac{\varepsilon_{zy}\left(6L_D+\sqrt{6}a\right)}{6n} - (i-1)\varepsilon_{zy}\left(L+\frac{b}{2}\right) - \frac{\varepsilon_{zmc3}(b+nL)}{2n} - \frac{\varepsilon_{zic}\left(6L_D+\sqrt{6}a\right)}{6n}\right) \pm L\frac{\Delta Y_{\mathrm{PSD2}}}{f} \\
&\quad + (-1)^{i-1}\left(-\varepsilon_{zir}\left(2L+\frac{b}{n}+\frac{b}{2}+\frac{6L_D+\sqrt{6}a}{3n}\right) + \delta_{xir} - \delta_{yir} - b\varepsilon_{zmrs1}\left(\frac{1}{n}-1\right) - \frac{\delta_{xmc3}}{2} - \delta_{xic}\right) \\
&\quad + (-1)^{i-1}\left(-\left(\varepsilon_{zmrs1}+\varepsilon_{zmrs2}\right)\left(L(1-n)+\left(L_D+\frac{\sqrt{6}}{6}a\right)\left(\frac{1}{n}-1\right)\right)\right) \\
\delta_{zy} &= (-1)^{i-1}\left(\frac{\Delta Z_{\mathrm{QD1}}}{2} + \frac{\varepsilon_{xy}\left(6L_D+\sqrt{6}a\right)}{6n} + (i-1)\varepsilon_{xy}\left(L+\frac{b}{2}\right) + \frac{\varepsilon_{xmc3}(nL+b)}{2n} + \frac{\varepsilon_{xic}\left(6L_D+\sqrt{6}a\right)}{6n}\right) \pm L\frac{\Delta Z_{\mathrm{PSD2}}}{f} \\
&\quad + (-1)^{i-1}\left(\varepsilon_{yir}\frac{b}{n} + \left(\varepsilon_{xir}+\varepsilon_{yir}\right)\left(\frac{b}{2}+\frac{6L_D+\sqrt{6}a}{6n}+L\right) + b\varepsilon_{ymrs1}\left(\frac{1}{n}-1\right) - \frac{\delta_{zmc3}}{2} - \delta_{zic}\right) \\
&\quad + (-1)^{i-1}\left(\varepsilon_{ymrs1}+\varepsilon_{xmrs2}\right)\left(L(1-n)+\left(L_D+\frac{\sqrt{6}}{6}a\right)\left(\frac{1}{n}-1\right)\right) \\
\varepsilon_{zy} &= (-1)^{i-1}\left(\frac{\Delta Y_{\mathrm{PSD1}}}{2f} - \varepsilon_{zic} - \frac{1}{2}\varepsilon_{PEz} + 2\varepsilon_{zir} - (n-1)\left(\varepsilon_{zmrs1}+\varepsilon_{zmrs2}\right)\right) \pm \frac{\Delta Y_{\mathrm{PSD2}}}{f} \\
\varepsilon_{xy} &= (-1)^{2-i}\left(\frac{\Delta Z_{\mathrm{PSD1}}}{2f} + \varepsilon_{xic} + \frac{1}{2}\varepsilon_{PEy} - \varepsilon_{xir} - \varepsilon_{yir} + (n-1)\left(\varepsilon_{ymrs1}+\varepsilon_{xmrs2}\right)\right) \pm \frac{\Delta Z_{\mathrm{PSD2}}}{f} \\
\varepsilon_{yy} &= (-1)^{i-1}\frac{\Delta Z_{\mathrm{QD1}} - \Delta Z_{\mathrm{QD2}} + 2\varepsilon_{PEy}\left(L+\frac{b+L_D}{n}+\frac{\sqrt{6}a}{6n}\right) - \delta_{zmc3} + \delta_{zmc4} + \left(\varepsilon_{xmc3}-\varepsilon_{xmc4}\right)\left(L+\frac{b}{n}\right)}{2h}.
\end{aligned}
\tag{6}
$$

In the above measurement model, δ_{xmc3} and δ_{zmc3} represent the position errors of the beam in the horizontal and vertical directions, respectively, caused by the manufacturing errors of CCR3. ε_{zmc3} and ε_{xmc3} represent the two non-parallel errors between the incident and reflected beams caused by the manufacturing errors of CCR3. δ_{zmc4} and ε_{xmc4} are the position errors of the light in the vertical direction caused by the manufacturing errors of CCR4 and the angle errors between the incident and reflected beams. b is the side length of the RAP.

3.2.3. Z-axis measurement model. Equation (7) shows the Z-axis 5DOF geometric errors measurement model. During Z-axis measurement, the beam is not influenced by refraction. Therefore, it is not necessary to consider the manufacturing errors of the RAP:

$$
\begin{aligned}
\delta_{yz} &= (-1)^{i-1}\left(\frac{\Delta Y_{\mathrm{QD1}}}{2} - \frac{(\varepsilon_{xz}+\varepsilon_{xic})\left(6L_D+\sqrt{6}a\right)}{6n} - (i-1)\,\varepsilon_{xz}\left(L+\frac{b}{2}\right) - \frac{\delta_{ymc5}}{2} - \delta_{yic}\right)\\
&\quad + (-1)^{i-1}\left(-\frac{(b+L)\,\varepsilon_{xmc5}}{2} - (\varepsilon_{xir}+\varepsilon_{zir})\left(L+\frac{b}{2}+\frac{6L_D+\sqrt{6}a}{6n}\right)\right) \pm L\frac{\Delta Y_{\mathrm{PSD2}}}{f}\\
\delta_{xz} &= (-1)^{i-1}\left(\frac{\Delta Z_{\mathrm{QD1}}}{2} + \frac{(\varepsilon_{yz}+\varepsilon_{yic})\left(6L_D+\sqrt{6}a\right)}{6n} + (i-1)\,\varepsilon_{yz}\left(L+\frac{b}{2}\right) - \frac{\delta_{xmc5}}{2} - \delta_{xic}\right)\\
&\quad + (-1)^{i-1}\left(\frac{(b+L)\,\varepsilon_{ymc5}}{2} + \delta_{xir} - \delta_{zir} + 2\varepsilon_{yir}\left(L+\frac{3b}{4}-\frac{6L_D+\sqrt{6}a}{6n}\right)\right) \pm L\frac{\Delta Z_{\mathrm{PSD2}}}{f}\\
\varepsilon_{xz} &= (-1)^{i-1}\left(\frac{\Delta Y_{\mathrm{PSD1}}}{2f} - \varepsilon_{xic} - \frac{1}{2}\varepsilon_{PEz} + \varepsilon_{xir} + \varepsilon_{zir}\right) \pm \frac{\Delta Y_{\mathrm{PSD2}}}{f}\\
\varepsilon_{yz} &= (-1)^{2-i}\left(\frac{\Delta Z_{\mathrm{PSD1}}}{2f} + \varepsilon_{yic} + \frac{1}{2}\varepsilon_{PEy} - 2\varepsilon_{yir}\right) \pm \frac{\Delta Z_{\mathrm{PSD2}}}{f}\\
\varepsilon_{zz} &= (-1)^{i-1}\frac{\Delta Z_{\mathrm{QD1}} - \Delta Z_{\mathrm{QD2}} - 2\varepsilon_{PEy}\left(b+L+\frac{6L_D+\sqrt{6}a}{6n}\right) + \delta_{xmc6} - \delta_{xmc5} - (b+L)\left(\varepsilon_{ymc6}-\varepsilon_{ymc5}\right)}{2h}.
\end{aligned}
\tag{7}
$$

δ_{ymc5} and δ_{xmc5} represent the position errors of the beam in the horizontal and vertical directions, respectively, owing to the manufacturing errors of CCR5. ε_{xmc5} and ε_{ymc5} represent the two non-parallel errors between the incident and reflected beams caused by the manufacturing errors of CCR5. Similarly, δ_{xmc6} and ε_{ymc6} represent the manufacturing errors of CCR6.

In summary, three linear axis geometric error comprehensive measurement models were established based on rigid body kinematics theory and the ray tracing method combined with the assumption of small angle error. The various types of systematic errors, including the manufacturing and installation errors of the CCR and RAP, error crosstalk, beam drift, non-parallelism errors between the two measured beams, and difference between the two measurement modes are reflected in the models. Among them, the measurement and compensation of beam drift have been deeply studied in the previous work [36]. By employing the proposed system to measure CNC machine tools and using the comprehensive measurement model to process raw data, high-precision geometric error evaluation results can be obtained. According to the expression form of the systematic error, the systematic error can be divided into three categories. The first category is the constant term systematic error. The second type is linear system error. The third type is the function item system error. In the process of data processing, the systematic error of the constant term can be eliminated by setting the initial measurement value to zero. The linear systematic error can be removed by the least square method or the least inclusion method. Finally, it is necessary to accurately measure the systematic error of the function term in order to eliminate each error. For example, the crosstalk of angular error to straightness error.

4. Numerical simulation with ZEMAX

The optical design software ZEMAX was used to verify the correctness of the measurement model. Owing to the space limitations, this section focuses on the numerical simulation of the position and manufacturing errors of the RAP. Other error terms in the measurement model, such as the manufacturing error and installation error of the CCR, have been verified previously [31]. As shown in figures 7(a) and (b), an ideal RAP was built with the incident beam parallel to the measurement axis. As illustrated in figure 7(c), footprint analysis was used to obtain the spot location and simulate four-quadrant detector QD in the actual system.

4.1. Analysis of angular error of RAP

In the numerical simulation process, the angular error of the RAP was set to 3.6″, the measuring distance L of the Y- and Z-axes varied from 0 to 800 mm, and the interval was 50 mm. Accordingly, the light spot deviated from its initial position on the footprint. Figure 8 shows the influence of the angular error of the RAP around the Z-axis on the Y measurement.

According to the Y- and Z-axis measurement models, the angular errors ε_{xir}, ε_{yir}, and ε_{zir} of the RAP and the distance L together cause a systematic error. This systematic error is composed of a constant term error and a linear error.

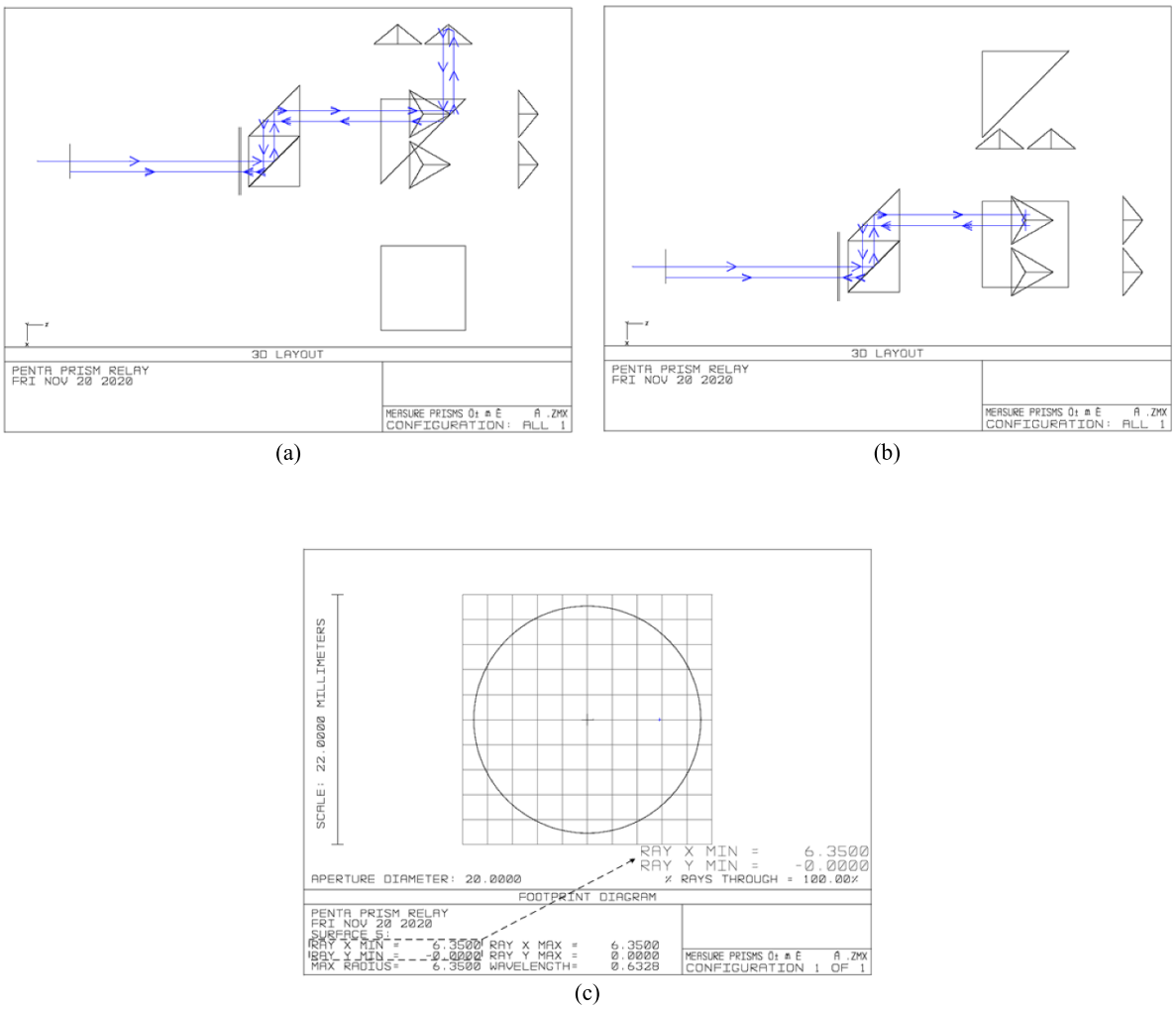

Figure 7. Measurement model simulation based on ZEMAX. (a) Ideal Y-axis measurement models; (b) ideal Z-axis measurement models; (c) spot position obtained by footprint analysis.

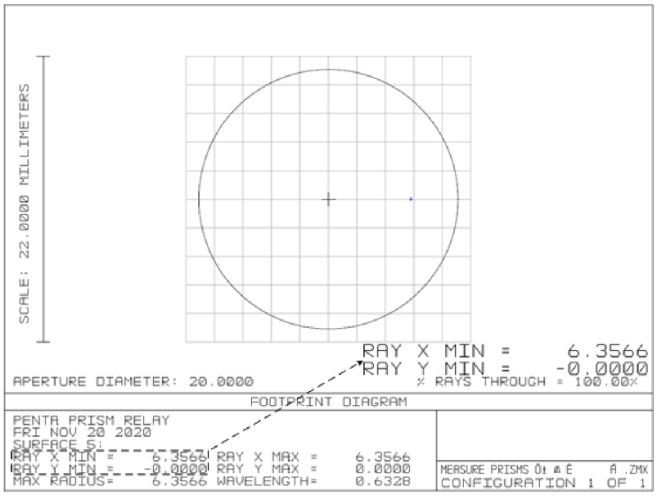

Figure 8. Simulation in the presence of $3.6''$ yaw installation error.

Usually, a constant system error can be eliminated by data processing. However, the linear system error affects not only the measurement range of the system, but also the measurement accuracy. Therefore, this section mainly analyzes the linear system errors caused by the angular errors of the RAP and the measured distance L. Equations (8) and (9) describe the

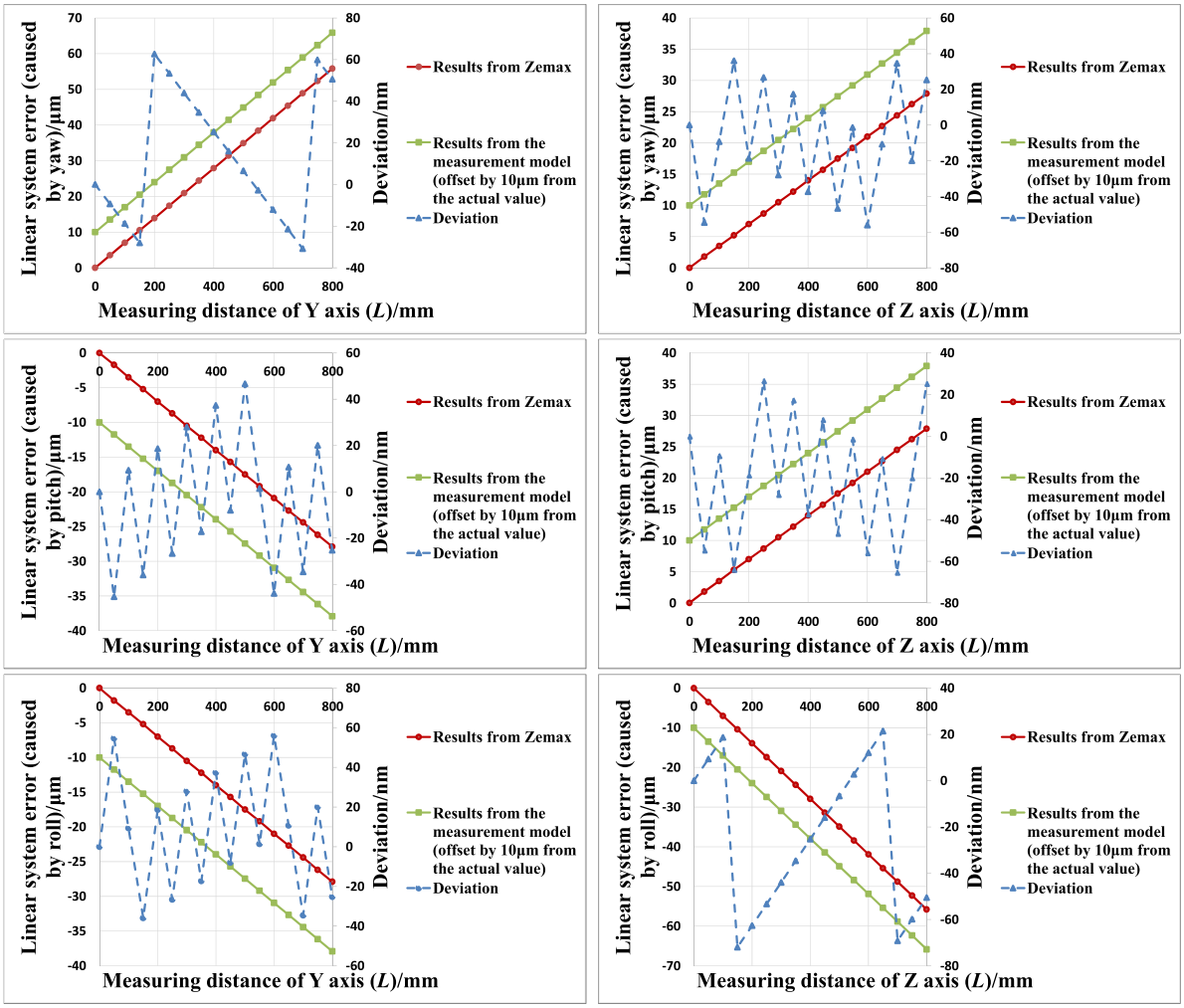

Figure 9. Comparison of the ZEMAX simulation and model calculation results.

effects of the linear system error term on the measurement of the straightness errors of the Y- and Z-axes, respectively:

$$\begin{aligned}\Delta Y_{\mathrm{QD1}} &= 4\varepsilon_{zir}L\\ \Delta Z_{\mathrm{QD1}} &= -2\left(\varepsilon_{xir}+\varepsilon_{yir}\right)L\end{aligned} \tag{8}$$

$$\begin{aligned}\Delta Y_{\mathrm{QD1}} &= 2\left(\varepsilon_{xir}+\varepsilon_{zir}\right)L\\ \Delta Z_{\mathrm{QD1}} &= -4\varepsilon_{yir}L.\end{aligned} \tag{9}$$

Figure 9 compares the ZEMAX simulation and model calculation results. To make the graph visible, the green line is offset by 10 μm from the actual value. These two sets of results are consistent. Through the simulation of the Y- and Z-axes, it can be seen that the yaw affects the horizontal straightness error of the Y-axis and the straightness error of the Z-axis in the Y-axis direction. The pitch affects the vertical straightness error of the Y-axis and the straightness error of the Z-axis in the Y-axis direction. Roll affects the vertical straightness error of the Y-axis and the straightness error of the Z-axis in the X-axis direction. The deviation between the simulation and model calculation results may be due to the fact that high-order systemic error was ignored in the measurement model.

4.2. Analysis of manufacturing error of RAP

In the numerical simulation process, the measuring distance L was 800 mm, and the interval was 50 mm. It was assumed that both manufacturing errors, ε_{zmrs1} and ε_{ymrs1}, between the reflective surface and right-angled surface of the RAP were $10.8''$. Figure 10 shows the displacement of the spot on the footprint caused by the manufacturing error of the RAP.

According to the measurement model, the influence of manufacturing errors on straightness varies with the measurement distance L. The measurement model can be simplified as follows:

$$\begin{aligned}Y_{\mathrm{QD1}} &= 2L(1-n)\varepsilon_{zmrs1}\\ Z_{\mathrm{QD1}} &= -2L(1-n)\varepsilon_{ymrs1}.\end{aligned} \tag{10}$$

Figure 11 compares the ZEMAX simulation and model calculation results. The green line is offset by 10 μm from the actual value to make the graph visible. These two sets of results are consistent and prove the validity of the measurement model.

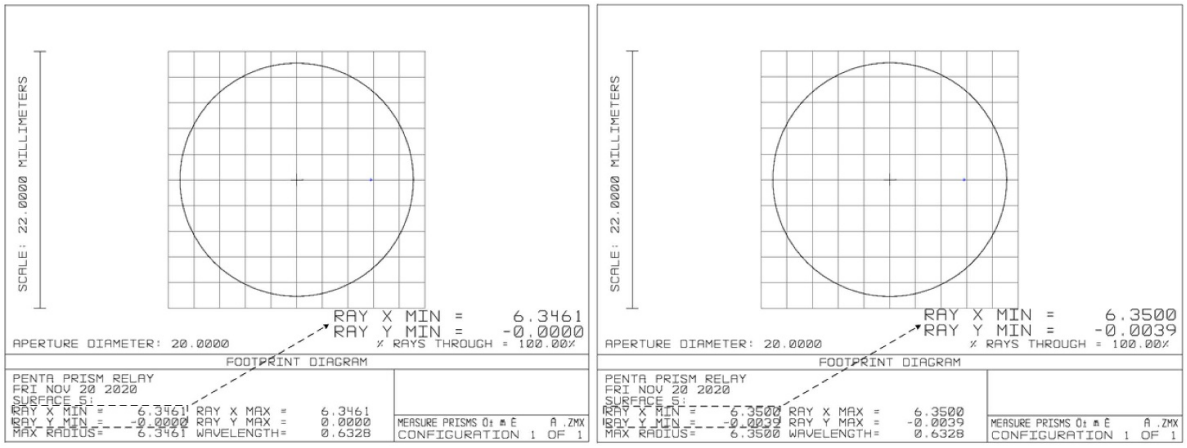

(a) (b)

Figure 10. Displacement of the light spot on the footprint caused by RAP manufacturing errors. (a) ε_{zmrs1} influence on horizontal straightness of the Y-axis. (b) ε_{ymrs1} influence on vertical straightness of the Y-axis.

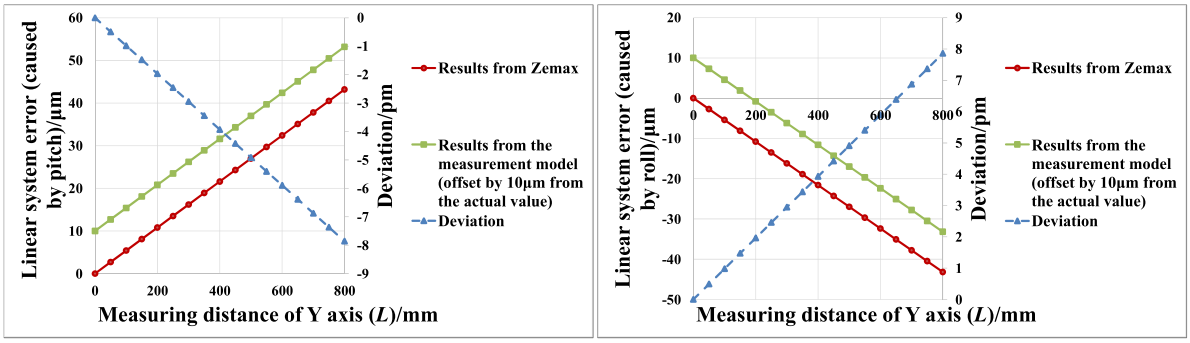

(a) (b)

Figure 11. Comparison between model calculation and ZEMAX simulation results. (a) ε_{zmrs1} influence on horizontal straightness of the Y-axis. (b) ε_{ymrs1} influence on vertical straightness of the Y-axis.

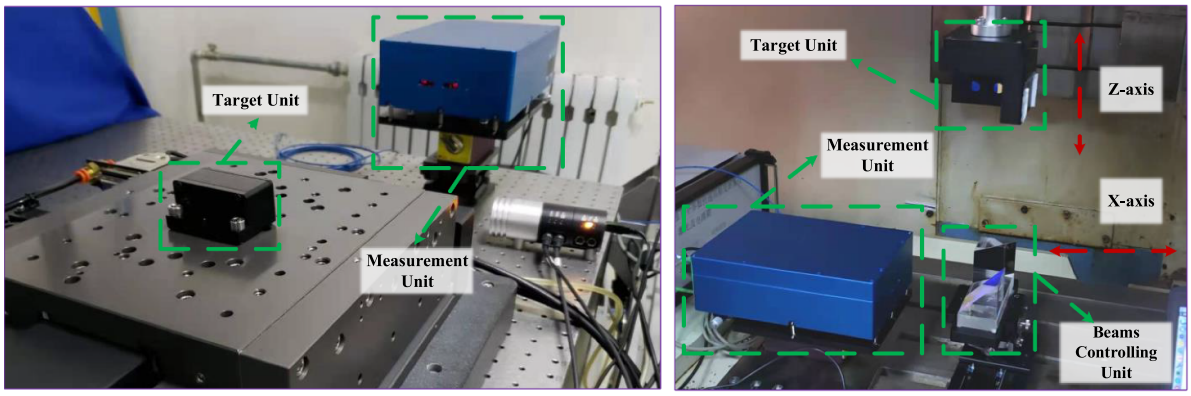

(a) b)

Figure 12. Repeatability and comparison experiments. (a) 6DOF geometric errors measurement; (b) squareness error measurement.

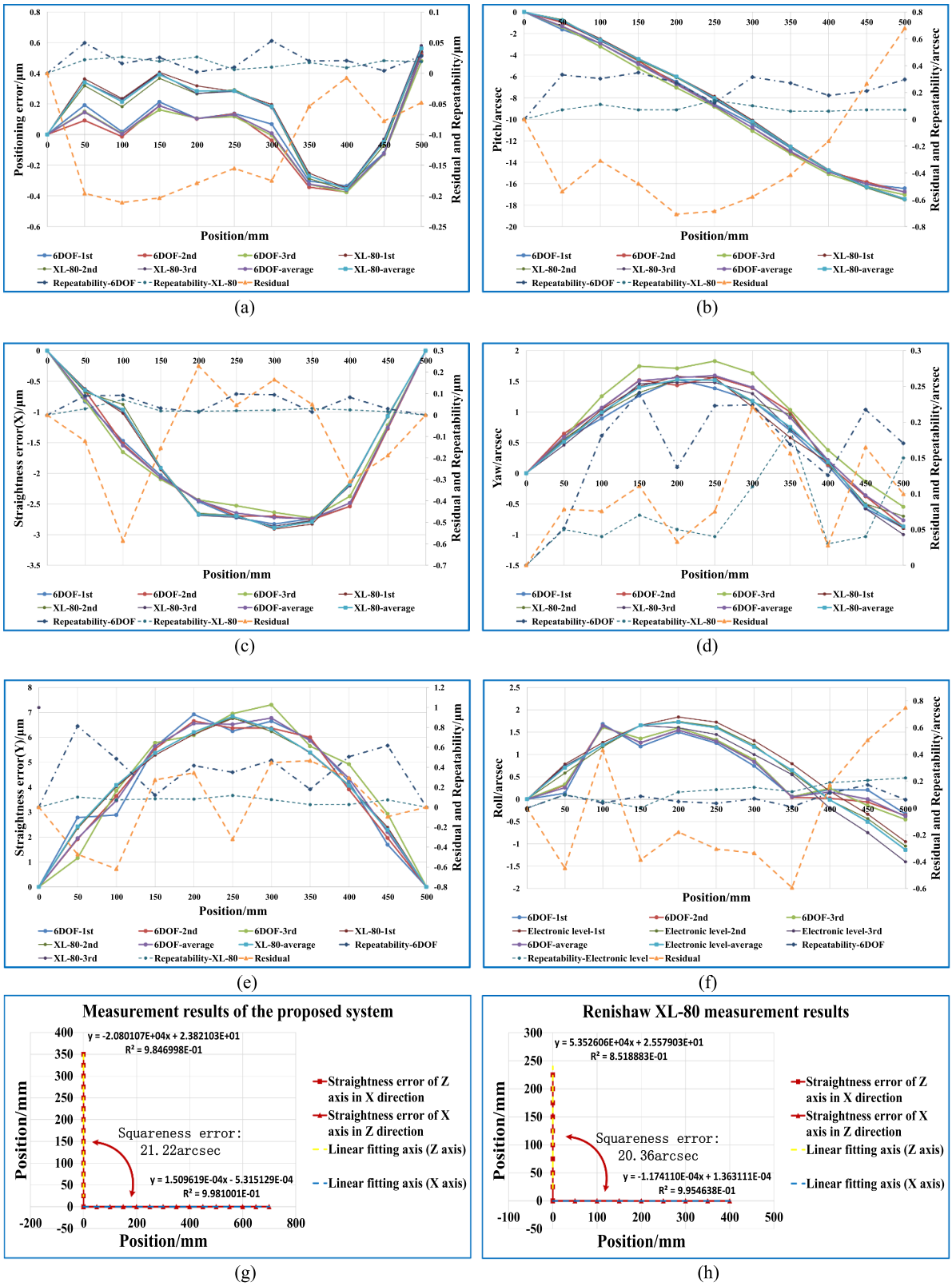

Figure 13. Results of repetitive and comparative experiments. (a) Positioning error; (b) pitch; (c) straightness error (*X*); (d) Yaw; (e) straightness error (*Y*); (f) roll; (g) squareness error measurement results of the proposed system; (h) squareness error measurement results of the Renishaw XL-80 measurement results.

Table 2. Repeatability and comparative experiment results obtained for the measurement system.

Parameter	Repeatability error—6DOF	Repeatability error—standard instrument	Maximum comparison deviation
Positioning error (nm)	±50	±30	70
Horizontal straightness error (μm)	±0.10	±0.07	0.23
Vertical straightness error (μm)	±0.81	±0.12	0.56
Pitch (″)	±0.35	±0.14	0.38
Yaw (″)	±0.24	±0.19	0.24
Roll (″)	±0.17	±0.23	0.69
Squareness error (″)	±0.29	±0.25	0.86

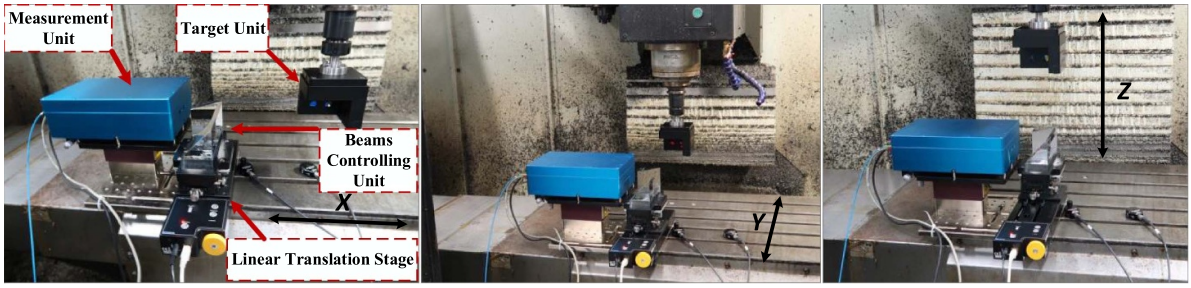

Figure 14. Three linear axis automatic measurement experiment. (a) *X*-, (b) *Y*- and (c) *Z*-axis measurement.

5. Experimental results and analysis

Experiments were conducted to verify the correctness of the comprehensive measurement model and the feasibility of the automatic system for three-linear-axis geometric error measurement.

5.1. Repeatability and comparison experiments

Figure 12 shows the 6DOF geometric errors measurement experiment of the air bearing linear guide and the squareness error measurement experiment between the *X*- and *Z*-axis of a CNC machine tool based on the proposed system. The experiment was repeated three times. The proposed measurement model was used to process the measurement data. Renishaw's XL-80 laser interferometer was utilized for the linear error, yaw, pitch and squareness error comparison. Outpost's electronic level was employed to compare the roll.

The repeatability of the three measurements was calculated using the formula (max − min)/2. The average value was compared with the measurement result obtained using the standard instrument, and contrast deviation was achieved. Figure 13 and table 2 respectively present the repeatability and comparison results. The results demonstrate that the system has high repeatability and measurement accuracy. The main cause of system repeatability errors are random errors, while the main cause of residual errors is the inconsistency of the measurement point between the measurement system and the standard instrument.

5.2. Automatic measurement of geometric errors of three-axis CNC machine tools

As shown in figure 14, in the actual processing environment, the measurement system was used to measure 21 geometric errors of the XYTZ-type three-axis CNC machine tool. The measurement and beam controlling units were fixed on the working platform of the machine tool through the Invar base plate. The target unit was fitted to the spindle. As shown in figure 14(a), when measuring the 6DOF geometric errors of the *X*-axis, the target unit was stationary, and the measurement and beam controlling units follow the *X* movement. As depicted in figure 14(b), to measure the 6DOF geometric errors of the *Y* axis, the linear translation stage was driven to add RAP1 to the optical path. The measurement unit and beam controlling unit moved along the *Y*-axis, and the target unit was stationary. As shown in figure 14(c), when measuring the 6DOF geometric errors of the *Z*-axis, the linear translation stage was driven to add RAP2 to the optical path. The measurement and beam-controlling units were stationary, and the target unit moved along the *Z*-axis. The test was repeated thrice under the same conditions. The comprehensive measurement model proposed in this study is used to process raw data. Figures 15–18 present the test results.

Table 3 shows the repeatability of the three measurements. The squareness error between the *X*- and *Y*-axes was −5.0″, the squareness error between the *X*- and *Z*-axes was −6.7″, and the squareness error between the *Y*- and *Z*-axes was −31.1″. The above measurement results truly reflect the performance of CNC machine tools.

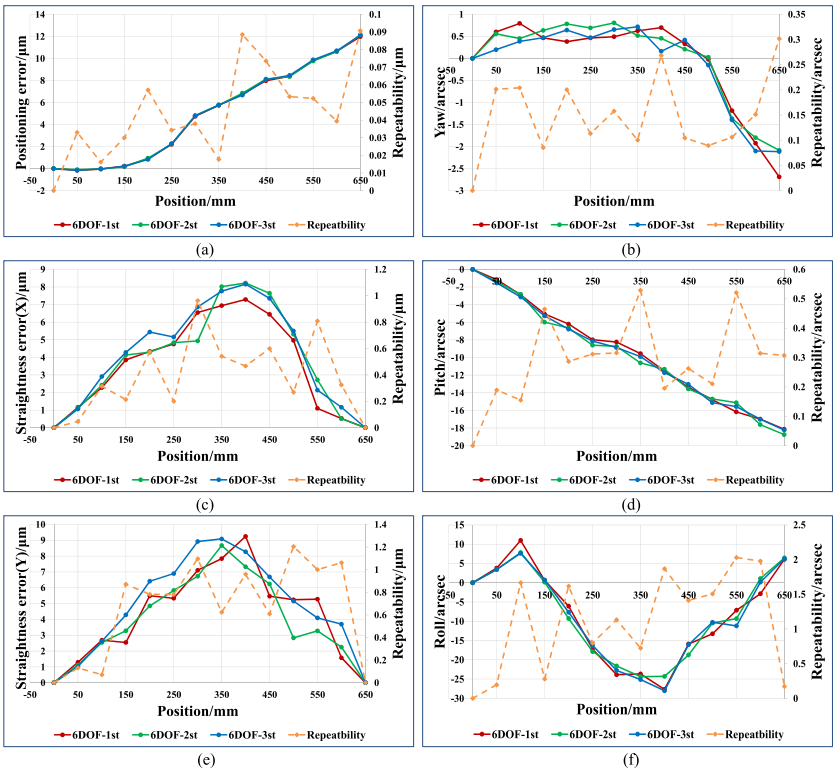

Figure 15. *X*-axis 6DOF geometric errors of a three-axis CNC machine tool. (a) Positioning error; (b) yaw; (c) horizontal straightness error; (d) pitch; (e) vertical straightness error; (f) roll.

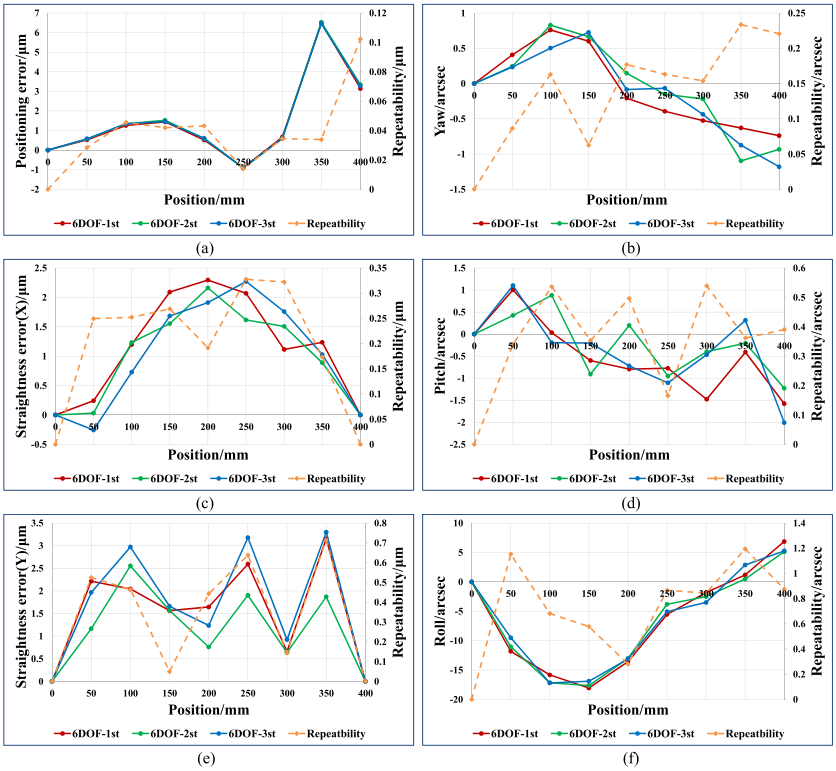

Figure 16. *Y*-axis 6DOF geometric errors of a three-axis CNC machine tool. (a) Positioning error; (b) yaw; (c) horizontal straightness error; (d) pitch; (e) vertical straightness error; (f) roll.

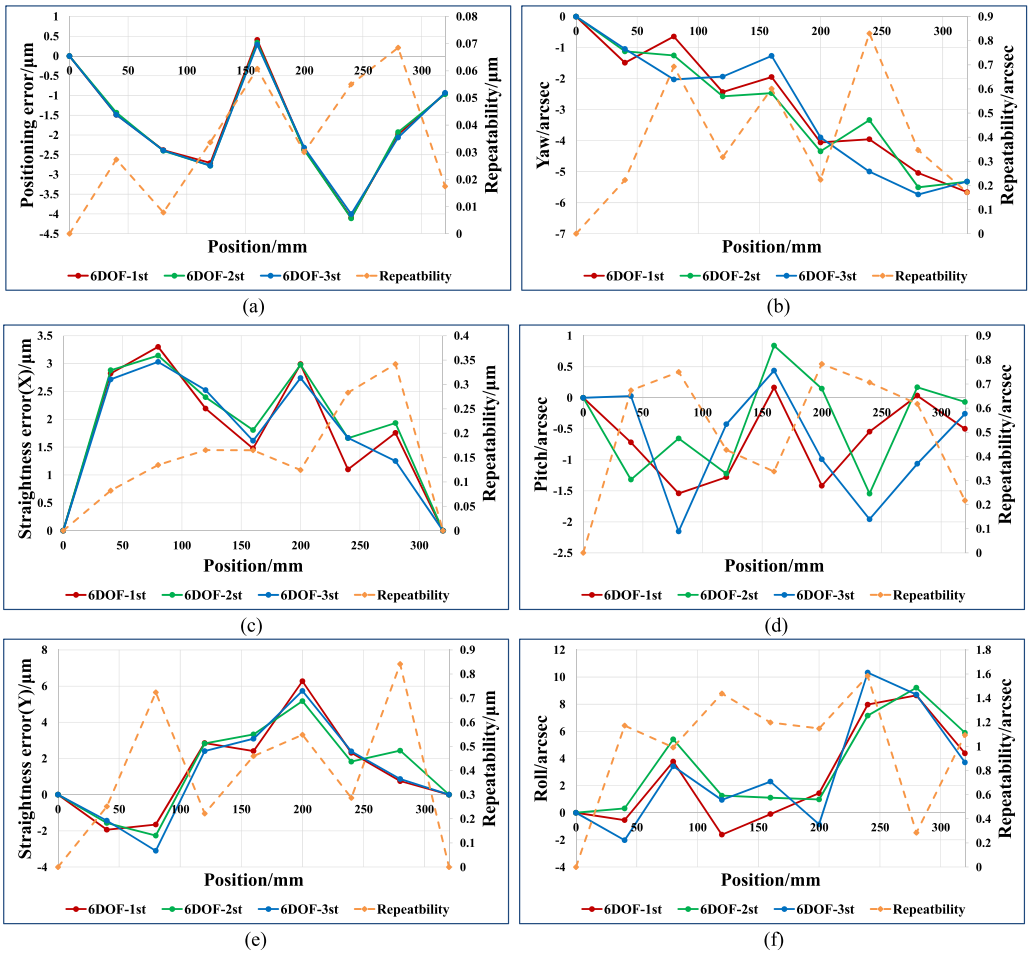

Figure 17. *Z*-axis 6DOF geometric errors of three-axis CNC machine tool. (a) Positioning error; (b) yaw; (c) horizontal straightness error; (d) pitch; (e) vertical straightness error; (f) roll.

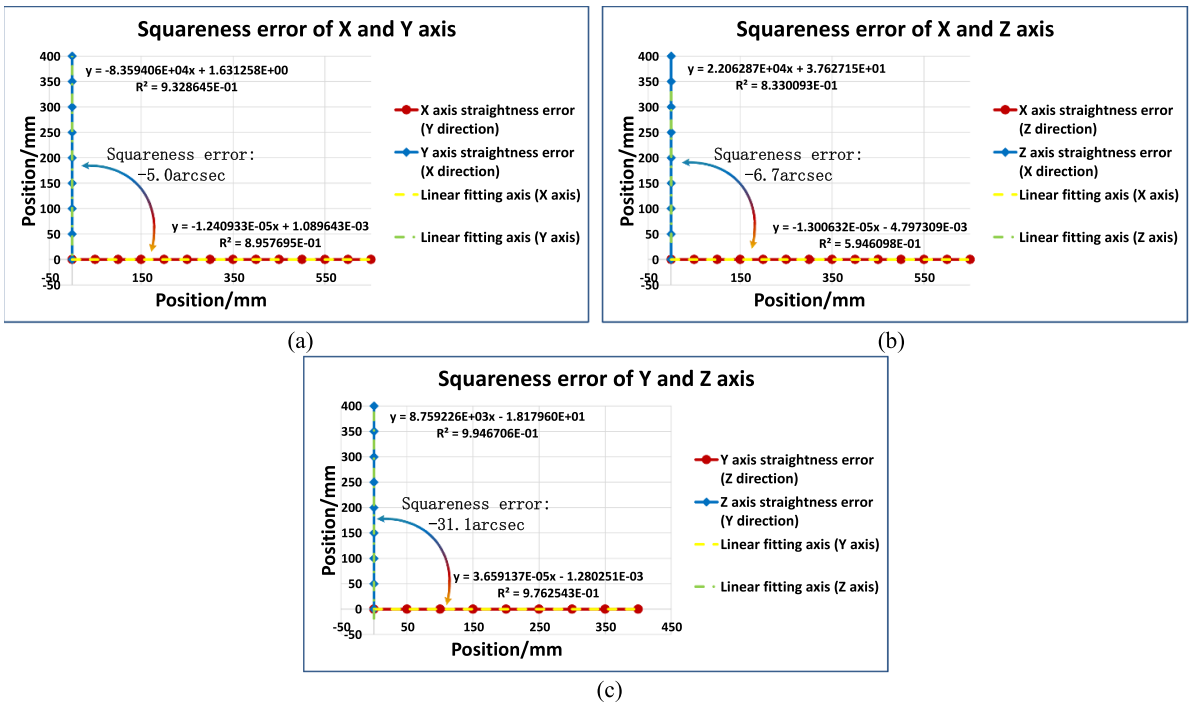

Figure 18. Squareness error measurement result. (a) Squareness error of *X* and *Y* axis; (b) Squareness error of *X* and *Z* axis; (c) Squareness error of *Y* and *Z* axis.

Table 3. Repeatability experiment results.

Parameter	*X*-axis Repeatability	*Y*-axis Repeatability	*Z*-axis Repeatability
Positioning error (nm)	±90	±10	±70
Horizontal straightness error (μm)	±0.96	±0.33	±0.34
Vertical straightness error (μm)	±1.21	±0.71	±0.84
Pitch (″)	±0.53	±0.23	±0.83
Yaw (″)	±0.30	±0.54	±0.78
Roll (″)	±2.03	±1.19	±1.58
Squareness error S_{xy} (″)	Repeatability: ±0.41		
Squareness error S_{xz} (″)	Repeatability: ±0.18		
Squareness error S_{yz} (″)	Repeatability: ±0.57		

6. Conclusion

This paper proposed a new method that can effectively and directly measure 21 geometric errors of the three linear axes of CNC machine tools. The 21 geometric errors of the three linear axes can be automatically measured with only one installation using the measurement system. Based on rigid body kinematics theory and the ray tracing method, a comprehensive error measurement model was established. The effects of system errors on the measurement accuracy were analyzed, including crosstalk errors, optical component manufacturing and installation errors, non-parallelism errors of the two measurement beams and the differences between measurement modes. ZEMAX optical design software was used to perform a numerical simulation to verify the correctness of the model. The measurement system and comprehensive measurement model are universally applicable to the linear axis geometric error measurement of all types of CNC machine tools. Repeatability and comparison experiments were conducted for the measurement system and verified the feasibility and effectiveness of the system and model. Finally, using the proposed measurement system and corresponding measurement model, the 21 geometric errors of an XYTZ CNC machine tool were measured three times in an actual processing workshop. The setup and measurement processes took approximately 35 min. Compared with the traditional single-parameter laser interferometer, the proposed measurement system has a high measurement efficiency.

Data availability statement

All data that support the findings of this study are included within the article (and any supplementary files).

Acknowledgment

This research was funded by the National Natural Science Foundation of the China-Major Program (51527806).

ORCID iD

Qibo Feng https://orcid.org/0000-0003-2854-044X

References

[1] Eskandari S, Arezoo B and Abdullah A 2013 Positional, geometrical, and thermal errors compensation by tool path modification using three methods of regression, neural networks, and fuzzy logic *Int. J. Adv. Manuf. Technol.* **65** 1635–49
[2] Schwenke H, Knapp W, Haitjema H, Weckenmann A, Schmitt R and Delbressine F 2008 Geometric error measurement and compensation of machines—an update *CIRP Ann. Manuf. Technol.* **57** 660–75
[3] Jiang Y J 2013 A methodology for systematic geometric error compensation in integrated inspection and machining *Appl. Mech. Mater.* **302** 535–40
[4] Ding S, Huang X, Yu C and Liu X 2016 Novel method for position-independent geometric error compensation of five-axis orthogonal machine tool based on error motion *Int. J. Adv. Manuf. Technol.* **83** 1069–78
[5] Ekinci T O and Mayer J 2007 Relationships between straightness and angular kinematic errors in machines *Int. J. Mach. Tools Manuf.* **47** 1997–2004
[6] Bringmann B, Küng A and Knapp W 2005 A measuring artefact for true 3D machine testing and calibration *CIRP Ann. Manuf. Technol.* **54** 471–4
[7] Trapet E, Martín J J A, Yagüe J A, Spaan H and Zeleny V 2006 Self-centering probes with parallel kinematics to verify machine-tools *Precis. Eng.* **30** 2 165–79
[8] Hong C and Ibaraki S 2013 Non-contact r-test with laser displacement sensors for error calibration of five-axis machine tool *Precis. Eng.* **37** 159–71
[9] Weikert S 2004 R-test, a new device for accuracy measurements on five axis machine tools *CIRP Ann. Manuf. Technol.* **53** 429–32
[10] Fan K C, Wang H, Shiou F J and Ke C W 2004 Design analysis and applications of a 3D laser ball bar for accuracy calibration of multiaxis machines *J. Manuf. Syst.* **23** 194–203
[11] Aguado S, Samper D, Santolaria J and Aguilar J J 2014 Volumetric verification of multiaxis machine tool using laser tracker *Sci. World J.* **2014** 959510
[12] Wang J and Guo J 2016 Geometric error identification algorithm of numerical control machine tool using a laser tracker *Proc. Inst. Mech. Eng.* B **230** 0954405415579856
[13] Holub M, Vetiska J, Bradac F and Vala M 2017 Application on-the-fly measurement of CNC machine tools *MM Sci. J.* **2017** 2085–9
[14] Deng M *et al* 2020 Geometric errors identification considering rigid-body motion constraint for rotary axis of multi-axis machine tool using a tracking interferometer *Int. J. Mach. Tools Manuf.* **158** 103625
[15] Li H, Zhang P, Deng M, Du Z * and Yang J 2020 Volumetric error measurement and compensation of three-axis machine tools based on laser bidirectional sequential step diagonal measuring method *Meas. Sci. Technol.* **31** 055201
[16] BS ISO 230-1 2012 *Test Code for Machine Tools–Part 1: Geometric Accuracy of Machines Operating Under*

No-Load or Quasi-Static Conditions (British Standards Institution)
[17] Okafor A C and Ertekin Y M 2000 Vertical machining center accuracy characterization using laser interferometer: part 1. Linear positional errors *J. Mater. Process. Technol.* **105** 394–406
[18] Okafor A C and Ertekin Y M 2000 Vertical machining center accuracy characterization using laser interferometer: part 2. angular errors *J. Mater. Process. Technol.* **105** 407–20
[19] Chen Y T, Lin W C and Liu C S 2017 Design and experimental verification of novel six-degree-of freedom geometric error measurement system for linear stage *Opt. Laser Eng.* **92** 94–104
[20] Liu C S, Lai J J and Luo Y T 2018 Design of a measurement system for six-degree-of-freedom geometric errors of a linear guide of a machine tool *Sensors* **19** 5
[21] Fan K C, Wang H Y, Yang H W and Chen L M 2014 Techniques of multi-degree-of-freedom measurement on the linear motion errors of precision machines *Adv. Opt. Technol.* **3** 375–86
[22] Huang Y, Fan K-C, Sun W and Liu S 2018 Low cost, compact 4-DOF measurement system with active compensation of beam angular drift error *Opt. Exp.* **26** 17185–98
[23] Wang W, Kweon S H, Hwang C S, Kang N C, Kim Y S and Yang S H 2009 Development of an optical measuring system for integrated geometric errors of a three-axis miniaturized machine tool *Int. J. Adv. Manuf. Technol.* **43** 701–9
[24] Gao W, Dejima S, Shimizu Y, Kiyono S and Yoshikawa H 2003 Precision measurement of two-axis positions and tilt motions using a surface encoder *CIRP Ann. Manuf. Technol.* **52** 435–8
[25] Li X, Shimizu Y, Ito T, Cai Y, Ito S and Gao W 2014 Measurement of six-degree-of-freedom planar motions by using a multiprobe surface encoder *Opt. Eng.* **53** 122405
[26] Kim J A, Kim K C, Bae E W, Kim S and Kwak Y K 2000 Six-degree-of-freedom displacement measurement system using a diffraction grating *Rev. Sci. Instrum.* **71** 3214–9
[27] Liu C H, Jywe W Y and Chen C K 2005 Development of a simple system for the simultaneous measurement of pitch, yaw and roll angular errors of a linear stage *Int. J. Adv. Manuf. Technol.* **26** 808–13
[28] Lee C B and Lee S K 2013 Multi-degree-of-freedom motion error measurement in an ultraprecision machine using laser encoder—review *J. Mech. Sci. Technol.* **27** 141–52
[29] Qibo F, Bin Z, Cunxing C, Cuifang K, Yusheng Z and Fenglin Y 2013 Development of a simple system for simultaneously measuring 6DOF geometric motion errors of a linear guide *Opt. Exp.* **21** 25805–19
[30] Cui C, Feng Q, Zhang B and Zhao Y 2016 System for simultaneously measuring 6DOF geometric motion errors using a polarization maintaining fiber-coupled dual-frequency laser *Opt. Exp.* **24** 6735–48
[31] Zhao Y, Zhang B and Feng Q 2017 Measurement system and model for simultaneously measuring 6DOF geometric errors *Opt. Exp.* **25** 20993
[32] Feng Q, Zhang B, Gao Z and Cui C 2018 6DOF error laser simultaneous measurement system with a single polarization maintaining fiber coupling and transmitting the dual-frequency laser *US Patent 9857161B2*
[33] Zheng F, Feng Q, Zhang B, Li J and Zhao Y 2020 A high-precision laser method for directly and quickly measuring 21 geometric motion errors of three linear axes of computer numerical control machine tools *Int. J. Adv. Manuf. Technol.* **109** 1–12
[34] Feng Q, Zhang B and Cui C 2018 Laser measurement system and method for measuring 21 GMES *US Patent 9982997B2*
[35] Jia P, Zhang B, Feng Q and Zheng F 2020 Simultaneous measurement of 6DOF motion errors of linear guides of CNC machine tools using different modes *Sensors* **20** 3439
[36] Zhao Y, Feng Q, Zhang B and Cui C 2016 Influence of beam radii on a common-path compensation method for laser beam drifts in laser collimation systems *Meas. Sci. Technol.* **27** 084013